Journal of the Mechanics and Physics of Solids 107 (2017) 145–159

Contents lists available at ScienceDirect

Journal of the Mechanics and Physics of Solids

journal homepage: www.elsevier.com/locate/jmps

Indentation of a stretched elastomer

Yue Zheng[a], Alfred J. Crosby[b], Shengqiang Cai[a,*]

[a] Department of Mechanical and Aerospace Engineering, University of California, San Diego, La Jolla, CA 92093, USA
[b] Polymer Science and Engineering Department, University of Massachusetts Amherst, Amherst, MA 01003, USA

ARTICLE INFO

Article history:
Received 28 March 2017
Revised 30 June 2017
Accepted 8 July 2017
Available online 10 July 2017

Keywords:
Indentation and hardness
Residual stress
Elastic material
Rubber material

ABSTRACT

Indentation has been intensively used to characterize mechanical properties of soft materials such as elastomers, gels, and soft biological tissues. In most indentation measurements, residual stress or stretch which can be commonly found in soft materials is ignored. In this article, we aim to quantitatively understand the effects of prestretches of an elastomer on its indentation measurement. Based on surface Green's function, we analytically derive the relationship between indentation force and indentation depth for a prestretched Neo-Hookean solid with a flat-ended cylindrical indenter as well as a spherical indenter. In addition, for a non-equal biaxially stretched elastomer, we obtain the equation determining the eccentricity of the elliptical contacting area between a spherical indenter and the elastomer. Our results clearly demonstrate that the effects of prestretches of an elastomer on its indentation measurement can be significant. To validate our analytical results, we further conduct correspondent finite element simulations of indentation of prestretched elastomers. The numerical results agree well with our analytical predictions.

1. Introduction

Indentation test has been intensively explored to measure mechanical properties of diverse materials ranging from metals (Corcoran et al., 1997; Ma and Clarke, 1995; Nix and Gao, 1998), ceramics (Gong et al., 1999; Pharr, 1998) to elastomers (Briscoe et al., 1998; VanLandingham et al., 2001) and biological tissues (Ebenstein and Pruitt, 2006; Oyen, 2010; Rho et al., 1997). In the experiment, indentation force is measured as a function of indentation depth, which can be used to assess fundamental mechanical properties of testing materials, such as elastic modulus and yield strength. Compared to many other mechanical testing methods including simple extension and compression tests, indentation test requires less or even no sample preparation, much smaller sample size and causes much less damage to the testing samples. In addition, by reducing the size of indenter, local mechanical properties of a heterogeneous material can be measured with high spatial resolution.

Recently, interest has been growing to use indentation test to characterize mechanical properties of gels and soft biological tissues (Constantinides et al., 2008; Ebenstein and Pruitt, 2004; Hu et al., 2012; Hu et al., 2010; Oyen, 2008). One salient feature of biological tissues and gels is that they are usually not in stress-free state. Large residual stress and strain can be commonly found in soft biological tissues (Fung, 1991; Fung and Liu, 1989; Rausch and Kuhl, 2013) as well as gels (Beebe et al., 2000; Hong et al., 2009). The residual stress and strain can be either isotropic or highly anisotropic (Amar and Goriely, 2005; Goriely et al., 2016; Marcombe et al., 2010). As a consequence, residual stress and strain may also exist in

* Corresponding author.
E-mail addresses: s3cai@ucsd.edu, shqcai@ucsd.edu (S. Cai).

http://dx.doi.org/10.1016/j.jmps.2017.07.008
0022-5096/

the sample for indentation test, though they can be partially or fully released through careful sample preparation. In particular, indentation tests have been recently explored to be directly conducted onto biological tissues without any sample preparation (Huang et al., 2005; Silver-Thorn, 1999; Vannah and Childress, 1996) to maintain their integrity and functionality. Therefore, measured relationship between indentation depth and indentation force should generally depend on both the mechanical properties and residual stress or strain state of testing samples. For instance, Zamir and Taber have shown that the calculated elastic modulus of soft biological tissues based on indentation test could be one order of magnitude higher than its true value if residual stress is ignored (Zamir and Taber, 2004). However, it is unclear how the residual stress or strain may quantitatively affect the indentation tests on soft materials.

According to our knowledge, Green, Rivlin, and Shield were the first who studied indentation of incompressible prestretched elastomers (Green et al., 1952). Later, the analysis was extended to compressible elastomers (Beatty and Usmani, 1975) and indenter with arbitrarily axisymmetric shape (Dhaliwal and Singh, 1978). Nevertheless, all the work was focused on the elastomer subject to equal-biaxial stretch, which greatly limits the application of their results. Filippova first studied indentation of a prestretched elastomer with non-equal biaxial prestretches (Filippova, 1978). To obtain analytical results of eccentricity of the contacting area between a spherical indenter and the elastomer as well as the indentation force as a function of indentation depth, the difference of two principle prestretches was assumed to be small. To study the effect of prestretch of an elastomer on its adhesion, Gay assumed deformation of elastomer stays in linear regime and took the prestretch into consideration by "mapping" the spherical indenter into an ellipsoidal one (Gay, 2000). However, the intuitive assumption has not been verified and may introduce significant errors.

Although indentation is generally a nonlinear problem, deformation in the material caused by indentation is typically small. Linear elasticity model was commonly adopted for the material in formulating indentation problem. In this article, we study indentation of an elastomer in a homogenously prestretched state. The prestretch in the elastomer can be arbitrarily large. However, following the commonly adopted assumption, additional deformation caused by indentation is assumed to be small. As a result, the problem can be regarded as a small deformation superimposed onto a finite deformation in a material. Following the method developed by Biot and Ogden (Biot, 1965; Ogden, 1997), we formulate the indentation of a prestretched elastomer with both flat-ended cylindrical indenter and spherical indenter in Section 2. To validate our analytical results, in Section 3, we conduct corresponding finite element simulations and compare the numerical results to our analytical predictions. Concluding remarks of our investigation are included in Section 4.

2. Analytical modeling

2.1. Surface Green's function for a biaxially stretched elastomer

Surface Green's function for a biaxially stretched elastomer occupying half space has been derived by Filippova (1978) and He (2008), in which the elastomer is taken to be a homogeneous, isotropic, and incompressible Neo-Hookean solid. Since we will use the derived surface Green's function to solve the current indentation problem in the article, we will briefly summarize the results obtained by Filippova and He in the following.

We first introduce a Cartesian coordinate (x_1, x_2, x_3) into the elastomer, which is bounded by the surface $x_3 = 0$, as shown in Fig. 1(a). The elastomer is under prestretch λ_1 and λ_2 along x_1 and x_2 directions. When a unit external force in x_j direction is applied onto the surface of the elastomer at $\boldsymbol{\xi} = (\xi_1, \xi_2, 0)$, the induced displacement in x_i direction at $\mathbf{x} = (x_1, x_2, 0)$ is defined as surface Green's function $\boldsymbol{G}_{ij}(\mathbf{x} - \boldsymbol{\xi})(i, j = 1, 2, 3)$. In the scenario that the additional strains induced by external surface forces are small, the incremental displacement field $u_i(\mathbf{x})$ in the elastomer resulted from any distributed loading can be obtained by linear superposition

In our following analysis, the contact between indenter and the elastomer is assumed to be frictionless. Therefore, surface Green's function component $\boldsymbol{G}_{33}(\mathbf{x} - \boldsymbol{\xi})$ is the only relevant one as given by Filippova (1978) and He (2008),

$$G_{33}\left(\mathbf{x} - \boldsymbol{\xi}\right) = \frac{\lambda_1^2\lambda_2^2(t + r)r}{2\pi\mu\left(t^3 + t^2r + 3tr^2 - r^3\right)}, \tag{1}$$

in which μ is shear modulus of the elastomer, and r and t are defined by

$$r = \sqrt{(x_1 - \xi_1)^2 + (x_2 - \xi_2)^2}, \tag{2}$$

$$t = \lambda_1\lambda_2\sqrt{\lambda_1^2(x_2 - \xi_2)^2 + \lambda_2^2(x_1 - \xi_1)^2}. \tag{3}$$

The normal surface displacement $u_3(\mathbf{x})$ caused by a general normal pressure distribution $p(\mathbf{x})$ could be determined through the integration:

$$u_3(\mathbf{x}) = \iint_S G_{33}\left(\mathbf{x} - \boldsymbol{\xi}\right)p\left(\boldsymbol{\xi}\right)d\xi_1 d\xi_2, \tag{4}$$

where S is the area with nonzero pressure.

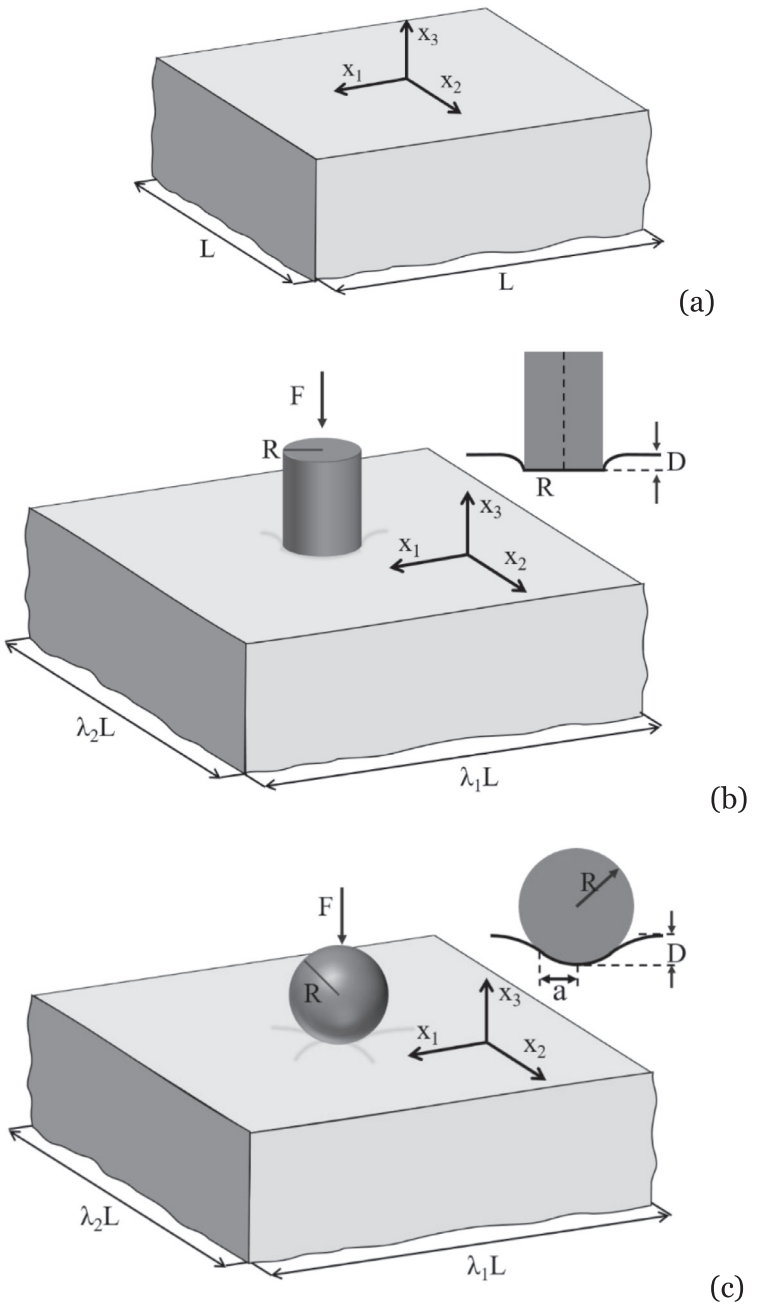

Fig. 1. Schematics of indentation of a prestretched elastomer. (a) A free-standing elastomer occupies half space. (b) A flat-ended cylindrical indenter is pressed onto the elastomer in a prestretched state. (c) A spherical indenter is pressed onto the prestretched elastomer. λ_1 and λ_2 are two lateral principle stretches applied onto the elastomer. R denotes the radius of both cylindrical and spherical indenter, F denotes indenting force, and D denotes indentation depth.

For the convenience of calculation in the following sections, we further simplify the expression in Eqs. (1)–(3) using the coordinate transformation:

$$\xi_1 = x_1 + r\cos\theta, \tag{5}$$

$$\xi_2 = x_2 + r\sin\theta. \tag{6}$$

In this polar coordinate, surface Green's function component $G_{33}(\mathbf{x}-\boldsymbol{\xi})$ can be rewritten as a function of r and θ:

$$G_{33}(r,\theta) = \frac{h(\theta)}{2\pi\mu r}, \tag{7}$$

where

$$h(\theta)=\frac{\lambda_1^2\lambda_2^2(g(\theta)+1)}{g(\theta)^3+g(\theta)^2+3g(\theta)-1}, \tag{8}$$

and

$$g(\theta)=\lambda_1\lambda_2\sqrt{\lambda_1^2\sin^2\theta+\lambda_2^2\cos^2\theta}. \tag{9}$$

2.2. Indentation of a prestretched elastomer with a flat-ended cylindrical indenter

We first formulate indentation of a prestretched elastomer with a flat-ended cylindrical indenter. The problem is sketched in Fig. 1(b). A flat-ended cylindrical indenter with radius R is pressed onto the surface of an elastomer, which is in a pre-stretched state with λ_1 and λ_2 as two principle stretches. Both indentation depth and indentation radius are assumed to be much smaller than the characteristic size of the elastomer. The contact between the indenter and the surface of elastomer is assumed to be frictionless. It has been proved that pressure distribution under a flat-ended cylindrical indenter takes the form (Willis, 1967):

$$p(\mathbf{x})=\left(p_0+p_1\frac{x_1}{R}+p_2\frac{x_2}{R}\right)\left(1-\frac{{x_1}^2}{R^2}-\frac{{x_2}^2}{R^2}\right)^{-1/2}, \tag{10}$$

where p_0, p_1 and p_2 are three constants to be determined.

In equilibrium state, the reaction force exerted onto the indenter can be calculated as:

$$F=\iint_S p(\mathbf{x})dx_1dx_2=2\pi\, p_0R^2. \tag{11}$$

During the indentation test, no torque is applied onto the indenter, which requires

$$\iint_S p(\mathbf{x})x_1dx_1dx_2=\frac{2\pi}{3}p_1R^3=0, \tag{12}$$

$$\iint_S p(\mathbf{x})x_2dx_1dx_2=\frac{2\pi}{3}p_2R^3=0. \tag{13}$$

Therefore, the pressure distribution in Eq. (10) can be further reduced to

$$p(\mathbf{x})=p_0\left(1-\frac{{x_1}^2+{x_2}^2}{R^2}\right)^{-1/2}, \tag{14}$$

with

$$p_0=\frac{F}{2\pi R^2}. \tag{15}$$

Recall Eq. (4), the magnitude of normal displacement on the surface of prestretched elastomer under flat-ended cylindrical indenter is given by

$$u_3(\mathbf{x})=\iint_S G_{33}(\mathbf{x}-\boldsymbol{\xi})p(\boldsymbol{\xi})d\xi_1d\xi_2, \tag{16}$$

in which S is the circular contacting area determined by the following equation:

$$\frac{{\xi_1}^2}{R^2}+\frac{{\xi_2}^2}{R^2}\le 1. \tag{17}$$

Using the coordinate transform shown in Eqs. (5)–(6), the pressure distribution $p(\boldsymbol{\xi})$ can also be expressed in the polar coordinate centered in $\mathbf{x}$ in the following form,

$$p(r,\theta)=p_0R\left[-r^2-2r(x_1\cos\theta+x_2\sin\theta)+\left(R^2-x_1^2-x_2^2\right)\right]^{-1/2}. \tag{18}$$

According to Eq. (17), the two limits of r are on the edge of the circular contacting area as,

$$r_{1,2}=-(x_1\cos\theta+x_2\sin\theta)\pm\sqrt{R^2-(x_1\sin\theta-x_2\cos\theta)^2}, \tag{19}$$

and θ ranges from 0 to π.

Therefore, the integration in Eq. (16) can be rewritten as,

$$u_3(\mathbf{x})=\int_0^{\pi}\int_{r_1}^{r_2}G_{33}(r,\theta)p(r,\theta)rdrd\theta. \tag{20}$$

The integration above results in a simple analytical form:

$$u_3(\mathbf{x}) = \frac{p_0 R}{2\mu} I, \tag{21}$$

where I only depends on λ_1 and λ_2 as

$$I = \int_0^{\pi} h(\theta) d\theta. \tag{22}$$

According to Eq. (21), the obtained normal displacement remains constant in the contacting area, in agreement with the uniform displacement boundary condition. For a flat-ended indenter, this constant displacement corresponds to the indentation depth D.

Substituting Eq. (15) into Eq. (21), we get the relation between indentation force and indentation depth:

$$F = \frac{4\pi\mu R}{I} D. \tag{23}$$

Pressure distribution can be also rewritten as

$$p(\mathbf{x}) = \frac{2\mu D}{IR}\left(1 - \frac{{x_1}^2 + {x_2}^2}{R^2}\right)^{-1/2}. \tag{24}$$

For an equal-biaxial stretched elastomer, $\lambda_1 = \lambda_2 = \lambda$, which reduces the above relation to a simpler form

$$F = \frac{4\mu R}{h} D, \tag{25}$$

$$h = \frac{\lambda^4\left(\lambda^3 + 1\right)}{\lambda^9 + \lambda^6 + 3\lambda^3 - 1}. \tag{26}$$

which agree with previous work (Beatty and Usmani, 1975; Dhaliwal and Singh, 1978). In particular, if $\lambda = 1$, $F = 8\mu RD$, which recovers the classical solution as shown in most elasticity textbooks (Bower, 2009).

Based on Eq. (23), the indentation force can be normalized as $F/\mu RD$. Through the normalization, indentation force becomes independent of indentation depth. If the elastomer is in a stress-free state before indentation, the normalized force should simply be a constant: 8. However, when the elastomer is prestretched before indentation, the normalized indentation force can greatly depend on the prestretched state as shown in Fig. 2(a). For a given prestretch ratio λ_2/λ_1, larger prestretch λ_1 results in larger indentation force. In particular, the normalized indentation force can decrease to zero for different prestretched states, which corresponds to Biot surface instability in a deformed elastomeric block. Based on linear stability analysis, the critical strain for Biot surface instability of a deformed elastomer can be given by $\lambda_2\sqrt{\lambda_1} = 0.543$ (Biot, 1963). The critical stretched states given by the above prediction are marked by cross in Fig. 2(a), which overlap with the prestretched state with zero indentation force. In addition, it has been recently discovered that before Biot surface instability happens, creases may form on the surface of a deformed elastomer. The critical conditions for the crease formation can be given by $\lambda_2\sqrt{\lambda_1} = 0.65$ (Hong et al., 2009), which are marked as circular points in Fig. 2(a). One important assumption in our formulation is that the additional strain caused by indentation is small. As expected, critical condition for Biot surface instability in an deformed elastomer can be captured by letting indentation force on the elastomer equal to zero. However, it is known that the additional strain caused by the crease formation is localized in space but finite in magnitude (Cai et al., 2012). Consequently, the condition for the onset of crease cannot be obtained through indentation analysis.

2.3. Indentation of a prestretched elastomer with a spherical indenter

We next formulate indentation of a prestretched elastomer with a spherical indenter, as sketched in Fig. 1(c). A rigid sphere with radius R is pressed onto the surface of an elastomer, which is in a prestretched state with λ_1 and λ_2 as two principle stretches. As before, both indentation depth and indentation radius are assumed to be much smaller than the characteristic size of the elastomer. The contact between indenter and the surface of elastomer is also assumed to be frictionless. For a spherical indenter in contact with an anisotropic elastic solid, it has been proved that the contacting area is an ellipse and the pressure distribution is (Willis, 1966)

$$p(\mathbf{x}) = p_0\left(1 - \frac{{x_1}^2}{a^2} - \frac{{x_2}^2}{b^2}\right)^{1/2}, \tag{27}$$

where p_0 is a constant, a and b are major and minor axes of the elliptical contacting area respectively. In the coordinate system, the center of contacting area coincides with the origin, and semi axes are along x_1 and x_2 directions.

The total force applied on the indenter is

$$F = \iint_S p(\mathbf{x}) dx_1 dx_2 = \frac{2\pi}{3} p_0 ab. \tag{28}$$

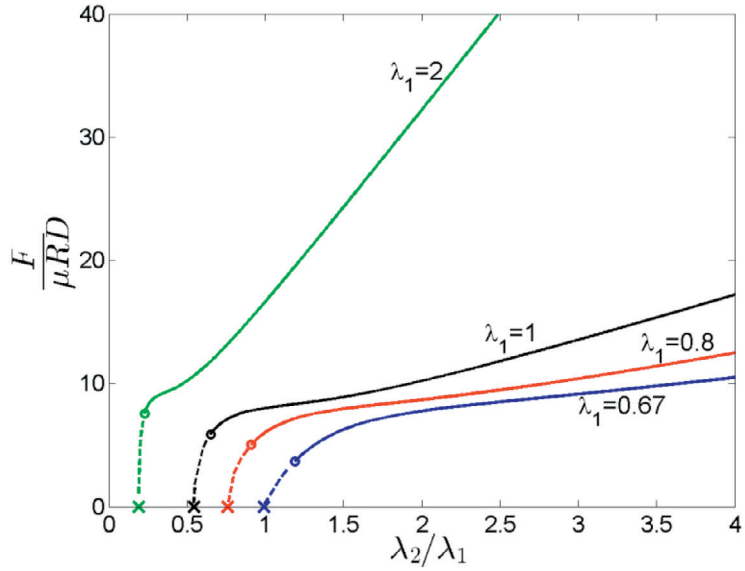

(a)

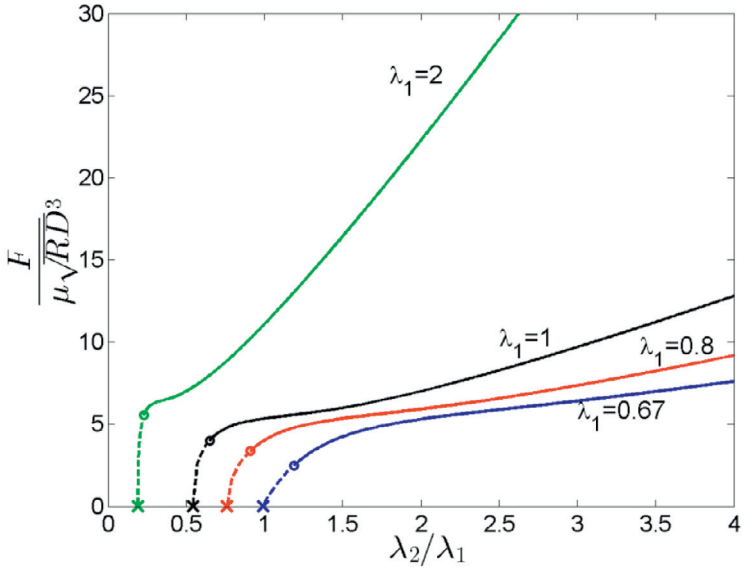

(b)

Fig. 2. Dependence of normalized indentation force on the prestretched state of a Neo-Hookean elastomer. Indentation force normalized by the indentation radius and indentation depth as shown in (a) flat-ended indenter and (b) spherical indenter is independent of indentation depth. For certain prestretched states, indentation force can decrease to zero, which corresponds to Biot surface instability of a deformed elastomer as marked by cross in both (a) and (b). Prestretched states for the onset of creases on the surface of the elastomers are marked by circular points in both (a) and (b).

Recall Eq. (4), the magnitude of normal displacement on the surface of the prestretched elastomer under spherical indenter is given by

$$u_3(\mathbf{x}) = \iint_S G_{33}(\mathbf{x}-\boldsymbol{\xi})\, p(\boldsymbol{\xi})\, d\xi_1 d\xi_2, \tag{29}$$

with elliptical contacting area:

$$\frac{{\xi_1}^2}{a^2} + \frac{{\xi_2}^2}{b^2} \le 1. \tag{30}$$

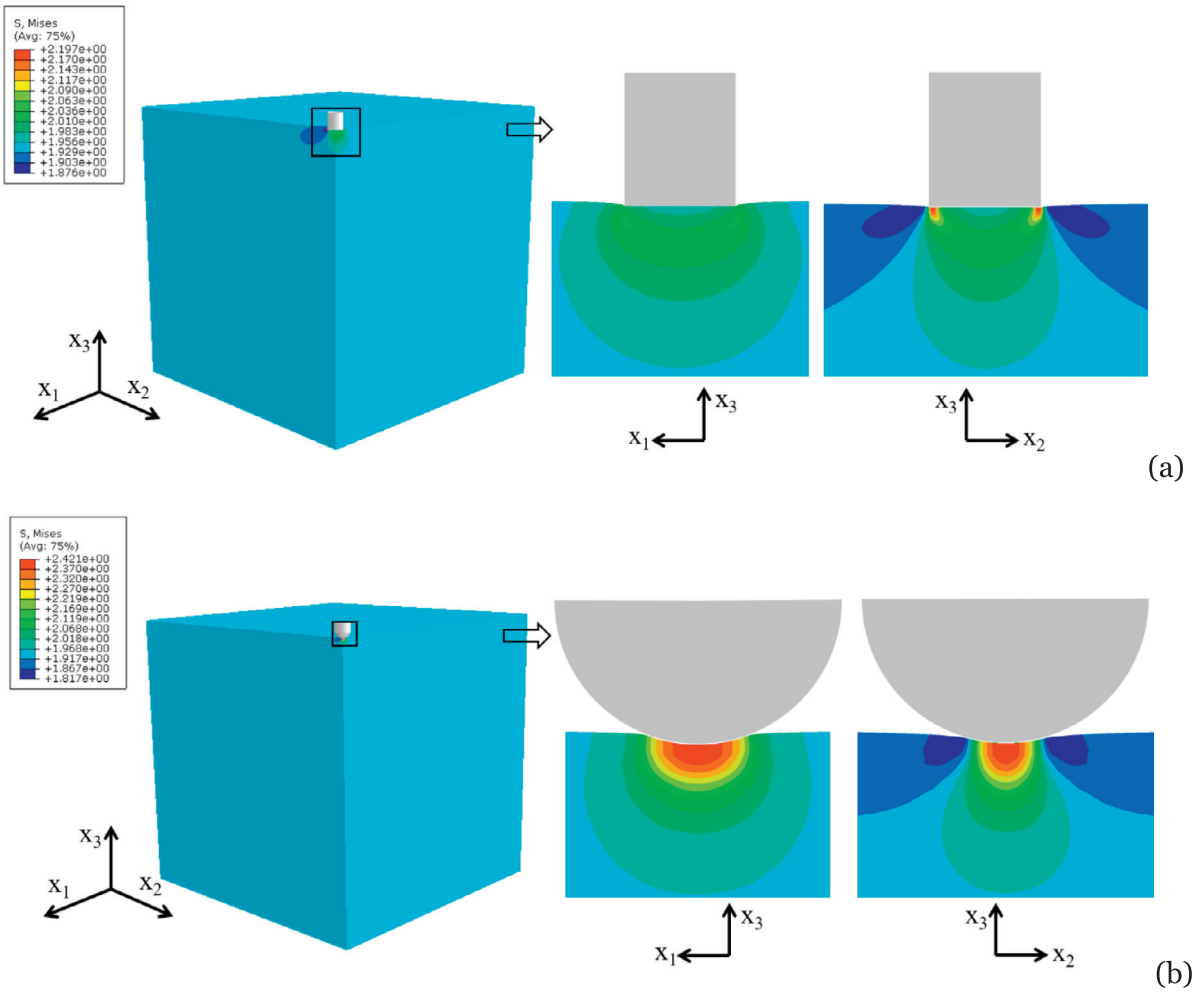

Fig. 3. Finite element simulations of indentation of a prestretched elastomer. Contour plot of the stress distribution around (a) flat-ended indenter and (b) spherical indenter for the prestretched state: $\lambda_1 = 0.8$, $\lambda_2 = 1.6$ and indentation depth $D = 0.1R$.

According to Eqs. (5)–(6), the pressure distribution $p(\boldsymbol{\xi})$ can be transformed to the polar coordinate:

$$p(r,\theta) = \frac{p_0}{ab}\left[-\left(b^2\cos^2\theta + a^2\sin^2\theta\right)r^2 - 2r\left(b^2x_1\cos\theta + a^2x_2\sin\theta\right) + \left(a^2b^2 - b^2x_1^2 - a^2x_2^2\right)\right]^{1/2}. \tag{31}$$

Therefore, Eq. (29) can be rewritten as

$$u_3(\mathbf{x}) = \int_0^{\pi}\int_{r_1}^{r_2} G_{33}(r,\theta)p(r,\theta)r\,dr\,d\theta, \tag{32}$$

where the integration limits r_1 and r_2 are given by the solution of the equation:

$$\frac{(x_1 + r_{1,2}\cos\theta)^2}{a^2} + \frac{(x_2 + r_{1,2}\sin\theta)^2}{b^2} = 1. \tag{33}$$

After integration, Eq. (32) can be finally simplified as:

$$u_3(\mathbf{x}) = \frac{bp_0}{4\mu}\left(I_0 - I_1\frac{{x_1}^2}{a^2} - I_2\frac{{x_2}^2}{a^2}\right), \tag{34}$$

with

$$I_0 = \int_0^{\pi}\frac{h(\theta)}{\left(1 - e^2\cos^2\theta\right)^{1/2}}d\theta, \tag{35}$$

$$I_1 = \int_0^{\pi}\frac{h(\theta)\sin^2\theta}{\left(1 - e^2\cos^2\theta\right)^{3/2}}d\theta, \tag{36}$$

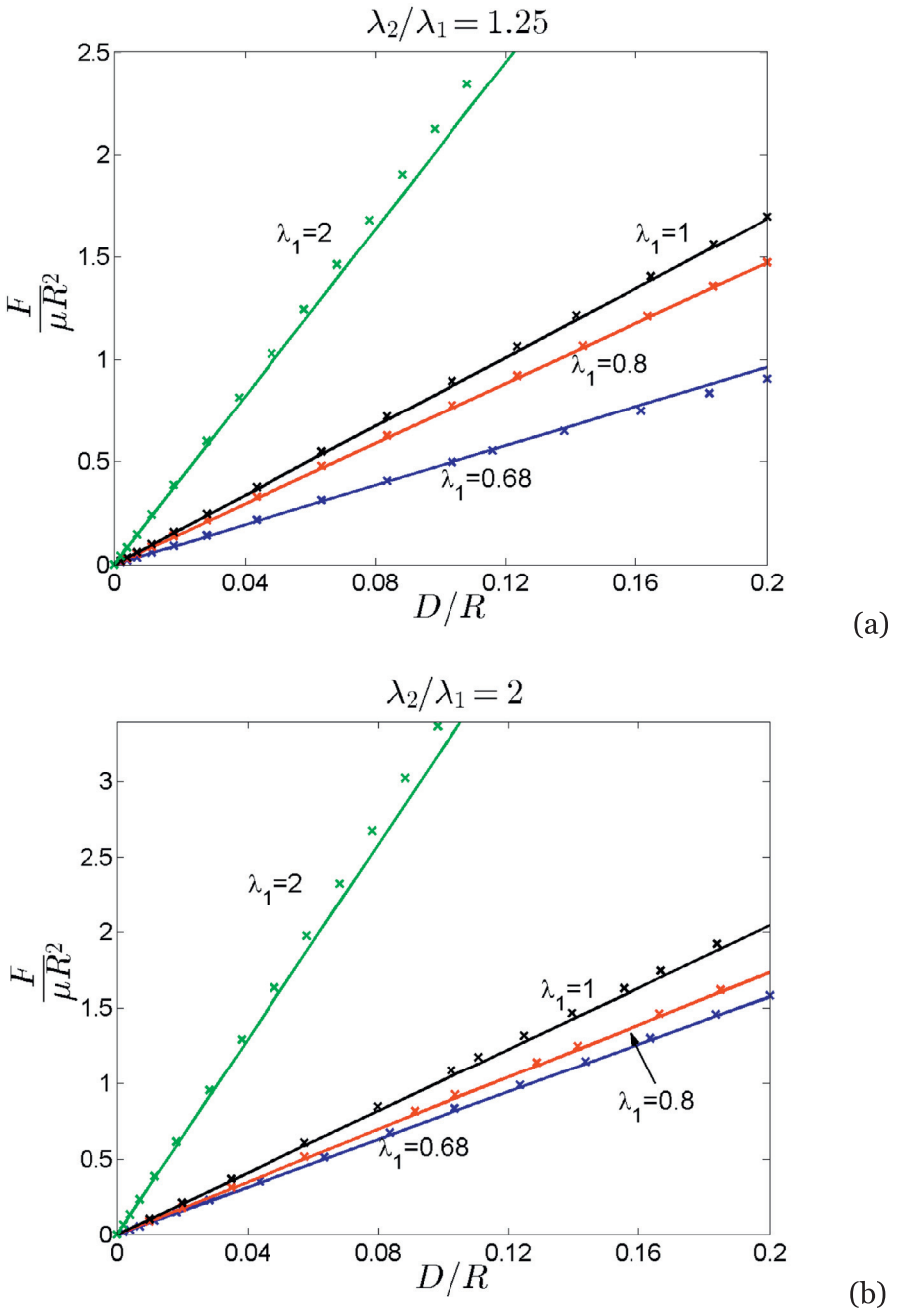

Fig. 4. Comparison between analytical prediction (solid line) and finite element computation (cross) of indentation force as a function of indentation depth for different prestretched state of an elastomer. The results are for flat-ended cylindrical indenter. In (a), ratio of the two lateral prestretches is set to be 1.25, and in (b), the ratio is set to be 2.

$$I_2 = \int_0^{\pi} \frac{h(\theta)\cos^2\theta}{\left(1 - e^2\cos^2\theta\right)^{3/2}} d\theta, \tag{37}$$

where $e = \sqrt{1 - (b/a)^2}$ denotes the eccentricity of the elliptical contacting area.

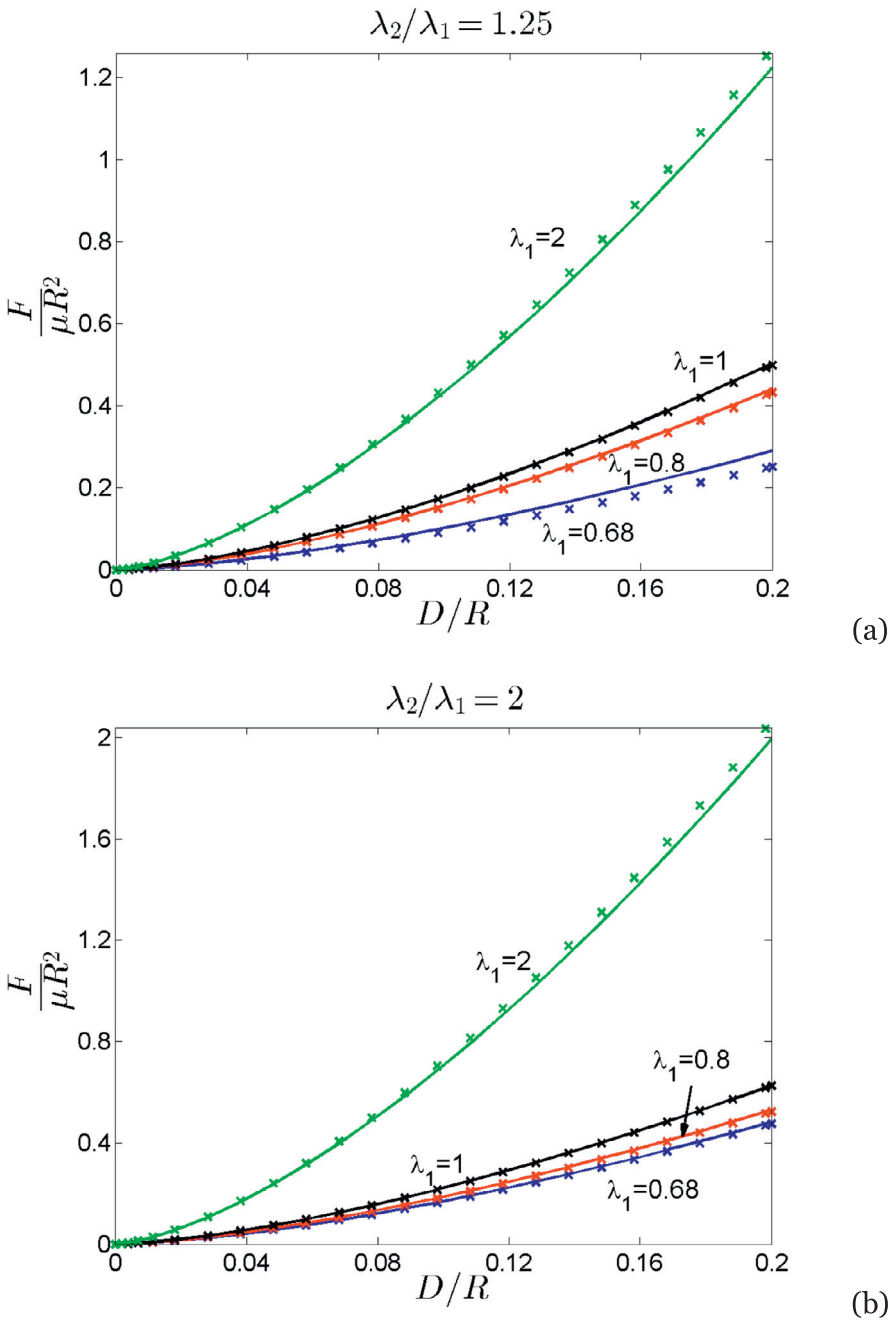

Fig. 5. Comparison between analytical prediction (solid line) and finite element computation (cross) of indentation force as a function of indentation depth for different prestretched state of the elastomer. The results are for spherical indenter. In (a), ratio of the two lateral prestretches is set to be 1.25, and in (b), the ratio is set to be 2.

For a spherical indenter with radius R and indentation depth D, the displacement on the surface of the elastomer imposed by the indenter can be approximated by,

$$u_3(\mathbf{x}) = D - \frac{1}{2R}x_1^2 - \frac{1}{2R}x_2^2. \tag{38}$$

Comparing Eq. (38) with (34), the calculated displacement agrees with the boundary condition when the following equations are satisfied

$$D = \frac{bp_0}{4\mu}I_0, \tag{39}$$

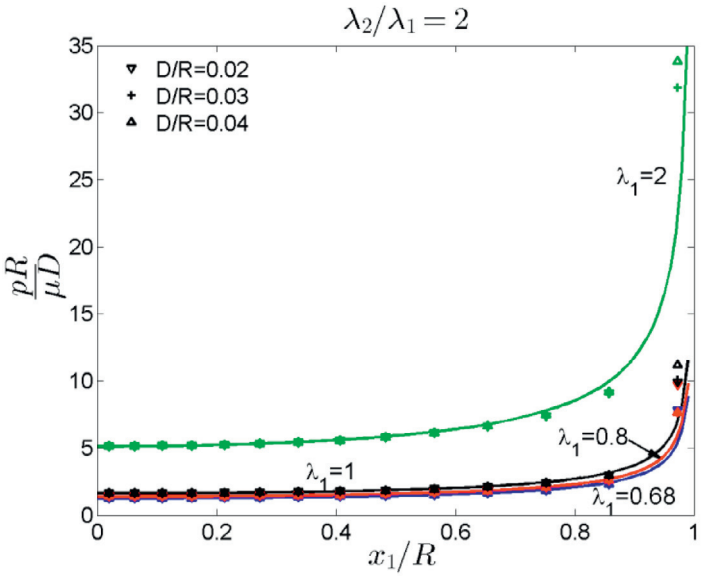

Fig. 6. Comparison between analytical prediction (solid line) and finite element simulation (markers) of contacting pressure between a flat-ended cylindrical indenter and biaxially prestretched elastomer. (a) and (b) show pressure distribution along x_1 and x_2 axis respectively. Simulation results at $D/R = 0.02$, $D/R = 0.03$, and $D/R = 0.04$ are marked with downward-pointing triangle, plus sign, and upward-pointing triangle markers. It is noted that through the normalization of indentation force and coordinates, the pressure distribution does not depend on indentation depth.

$$\frac{1}{2R} = \frac{bp_0}{4a^2\mu} I_1, \tag{40}$$

$$\frac{1}{2R} = \frac{bp_0}{4a^2\mu} I_2. \tag{41}$$

Eqs. (40) and (41) require $I_1 = I_2$, which determines the eccentricity of elliptical contacting area:

$$\int_0^{\pi} \frac{h(\theta)\left(\cos^2\theta - \sin^2\theta\right)}{\left(1 - e^2\cos^2\theta\right)^{3/2}} d\theta = 0, \tag{42}$$

which clearly shows that the eccentricity of elliptical contacting area is independent of indentation depth.

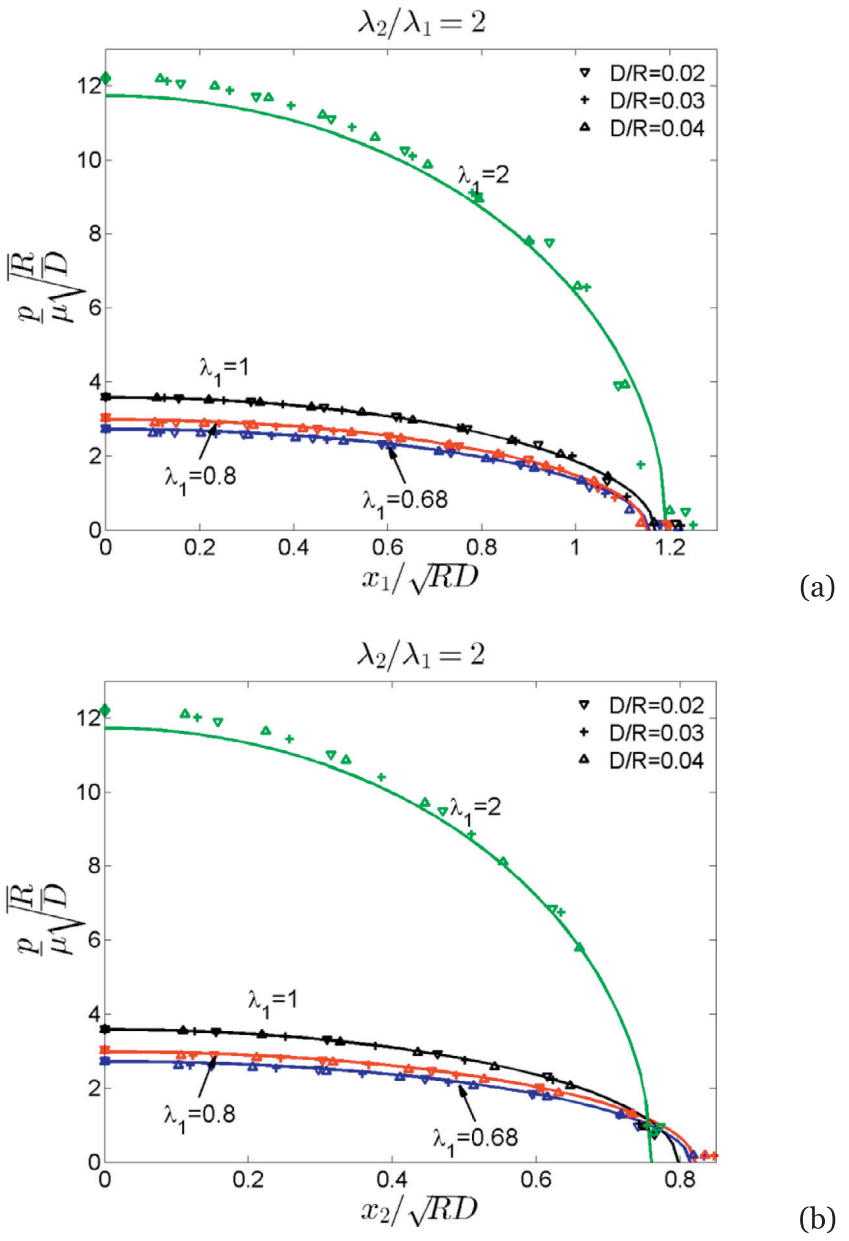

Fig. 7. Comparison between analytical prediction (solid line) and finite element simulation (markers) of contacting pressure between a spherical indenter and biaxially prestretched elastomer. (a) and (b) show pressure distribution along x_1 and x_2 axis respectively. Simulation results at $D/R = 0.02$, $D/R = 0.03$, and $D/R = 0.04$ are marked with downward-pointing triangle, plus sign, and upward-pointing triangle markers. It is noted that through the normalization of indentation force and coordinates, the pressure distribution does not depend on indentation depth.

It can be noticed that $I_0 = I_1 + (1 - e^2)I_2$ from Eqs. (35)–(37). Combing this relationship with Eqs. (39)–(41), we can further obtain that

$$a = \sqrt{\frac{2RD}{2 - e^2}}. \tag{43}$$

A combination of Eqs. (28) and (39) gives,

$$F = \frac{8\pi\mu aD}{3I_0}. \tag{44}$$

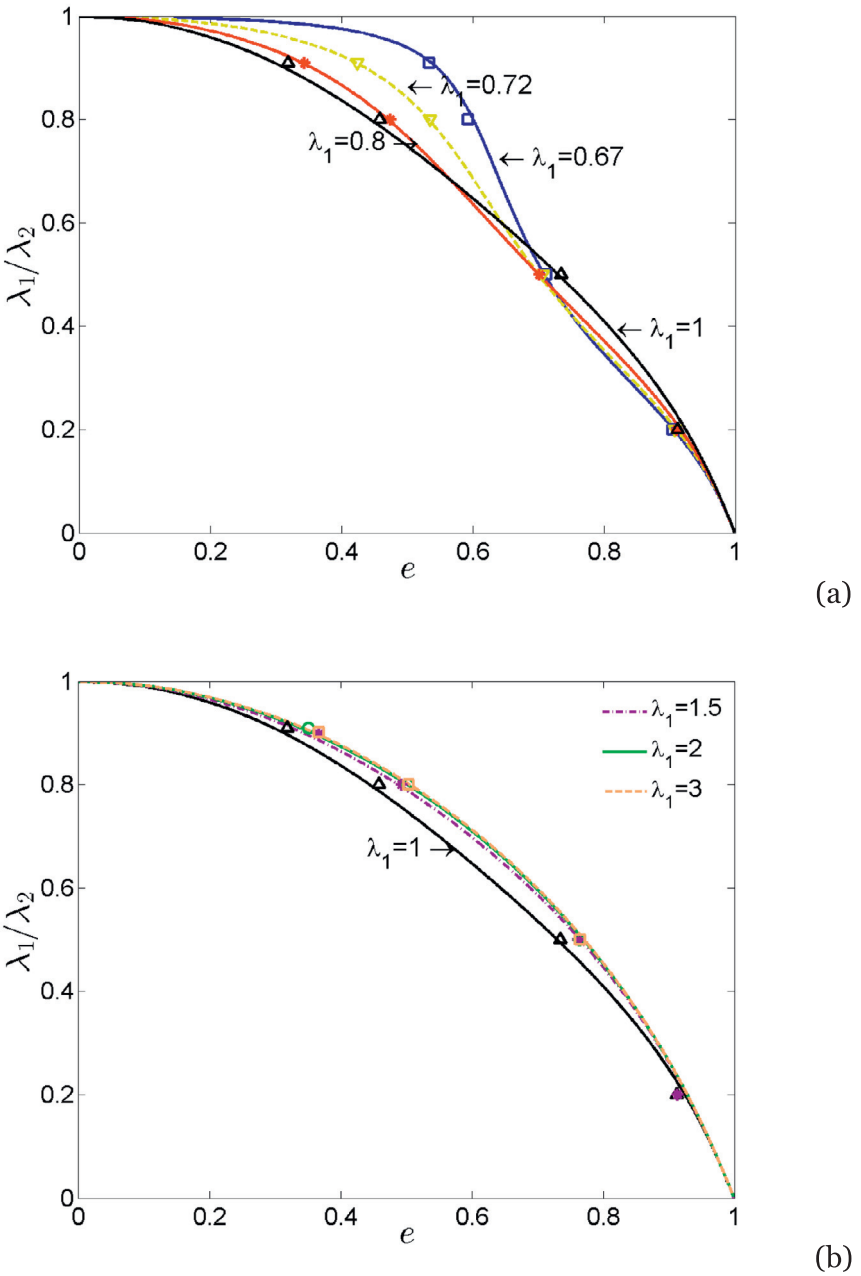

Fig. 8. For a spherical indenter, the contacting area between indenter and prestretched elastomer is generally elliptical. The figures (a) and (b) illustrate the dependence of eccentricity: e on the prestretched state of the elastomer. In (a), λ_1 is set to be smaller than one. In (b), λ_1 is set to be larger than one. In the figures, curves are analytical predictions and markers are taken from finite element simulations. Different λ_1 are specified with different colors.

Substituting Eq. (43) into Eq. (44), we obtain that

$$F = \frac{8\pi\mu}{3I_0}\sqrt{\frac{2R}{2-e^2}}D^{\frac{3}{2}}. \tag{45}$$

Eq. (45) shows that indentation force depends on the indentation depth to 3/2 power, which is exactly the same as no prestretched case.

Pressure distribution can be rewritten by plugging Eqs. (28), (43), and (45) into Eq. (27):

$$p(\mathbf{x}) = \frac{4\mu}{I_0}\sqrt{\frac{(2-e^2)D}{2(1-e^2)R}}\left(1-\frac{(2-e^2){x_1}^2}{2RD}-\frac{(2-e^2){x_2}^2}{(1-e^2)2RD}\right)^{1/2}. \tag{46}$$

The elliptical contacting area between the indenter and the elastomer can be given by: $A=\pi ab$, which can be further computed using Eq. (43):

$$A = \pi\frac{2\sqrt{1-e^2}}{2-e^2}RD. \tag{47}$$

For equal-biaxially stretched elastomer, $\lambda_1=\lambda_2=\lambda$, due to the symmetry, $a=b$ and $a^2=RD$, which reduce the Eq. (45) to a simpler form

$$F = \frac{8\mu R^{1/2}}{3h}D^{3/2}, \tag{48}$$

$$h = \frac{\lambda^4(\lambda^3+1)}{\lambda^9+\lambda^6+3\lambda^3-1}. \tag{49}$$

which agree with result of Green et al., (1952). In particular, if $\lambda=1$, $F=\frac{16\mu R^{1/2}D^{3/2}}{3}$, the classical elasticity solution is recovered.

Based on Eq. (45), the indentation force can be normalized as $F/\mu R^{1/2}D^{3/2}$. Through the normalization, indentation force becomes independent of indentation depth. If the elastomer is in a stress-free state before indentation, the normalized force is a constant: 16/3. However, when the elastomer is prestretched before indentation, the normalized indentation force can greatly depend on the prestretched state as shown in Fig. 2(b). For a given prestretch ratio λ_2/λ_1, larger stretch λ_1 results in larger indentation force. Similar to Section 2.2, the normalized indentation force can also decrease to zero for different prestretched state, which corresponds to the same critical condition of Biot instability (Biot, 1963). Similarly, the critical conditions for the crease formation are marked as circular points in Fig. 2(b).

3. Finite element simulation

To validate the analytical model, we simulate indentation of prestretched elastomers using commercial finite element software ABAQUS (Version 6.12). Three dimensional models are set up in ABAQUS/Standard as shown Fig. 3: A flat-ended cylindrical/spherical indenter is in contact with a block of elastomer. The indenter is assumed to be rigid and the elastomer block is set to be incompressible Neo-Hookean material. Considering the symmetric geometry and loading conditions, we only simulate a quarter of the elastomer, the width W and height H of which are set to be 50 times of the indenter radius. The four side planes of the block are fixed in their normal directions, and bottom plane is fixed in the vertical direction; A downward vertical displacement is applied on the indenter. The contact between the indenter and elastomer block is set to be frictionless. We prestretch the elastomer along x_1 and x_2 directions by applying initial stresses on it. Before indentation, the upper surface of the block remains flat, and the indenter is in contact with it with no applied force. The block is meshed with 8 node linear hybrid brick elements with reduced integration(C3D8RH). There are approximately 300,000 elements in a quarter of the elastomer block as shown in Fig. 3. Around the contacting area, the mesh is further refined and the length of the element side is 0.5%–1% of the indenter diameter.

Load-displacement curves obtained from ABAQUS are compared to theoretical predictions as shown in Fig. 4 for a flat-ended cylindrical indenter and Fig. 5 for a spherical indenter. In the simulations, several different prestretched states are considered: $\lambda_1=0.68$, $\lambda_1=0.8$, $\lambda_1=1$, and $\lambda_1=2$ with $\lambda_2/\lambda_1=1.25$ or $\lambda_2/\lambda_1=2$. Both Figs. 4 and 5 clearly show dramatic effects of prestretches on the indentation measurements. In addition, the agreement between FEM simulations and our analytical predictions is generally good. With the increase of indentation depth, some deviation can be seen between FEM simulations and our analytical results, which may be due to the increase of the additional strain in the elastomer caused by indentation. Based on the comparison between the simulation results and our analytical predictions shown in Figs. 4 and 5, $D/R<0.1$ can be regarded as the range, within that analytical predictions of load-displacement results could be used.

Fig. 6 shows the contacting pressure between a flat-ended cylindrical indenter and biaxially prestretched elastomer. Fig. 6(a) and (b) present pressure distribution along radius coincident with x_1 and x_2 axis respectively. According to Eq. (24), normalized pressure $pR/\mu D$ is independent of indentation depth D. Several prestretched states with different λ_1 and λ_2/λ_1 are considered. The analytical predictions are represented by solid lines and finite element simulations when $D/R=0.02$, $D/R=0.03$, $D/R=0.04$ are marked with downward-pointing triangle, plus sign, and upward-pointing triangle. As the figure shows, simulation results fit well with the predictions of pressure distribution.

Fig. 7 shows the contacting pressure between a spherical indenter and biaxially prestretched elastomer, where (a) and (b) correspond to pressure distribution along semi axis a and b of contacting area. According to Eq. (46), the relation between normalized pressure $\frac{p}{\mu}\sqrt{\frac{R}{D}}$ and normalized coordinates $\mathbf{x}/\sqrt{RD}$ is independent of indentation depth D. The same

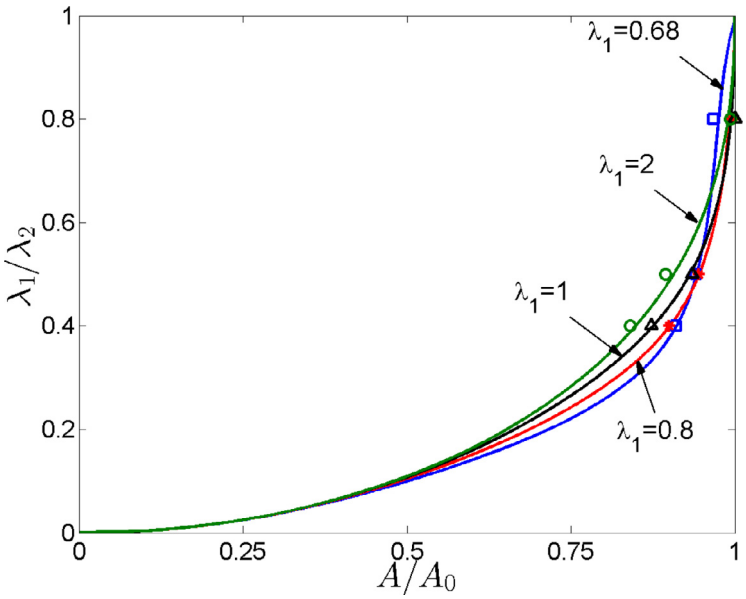

Fig. 9. Normalized contacting area between a spherical indenter and a prestretched elastomer depends on the prestretched state of the elastomer. In the figure, solid lines and markers are analytical and numerical simulation results, respectively.

prestretched states as Fig. 6 are considered. The analytical predictions are represented by solid lines and finite element simulations ranging from $D/R = 0.02$ to $D/R = 0.04$ are represented by markers. As the plots show, simulation results fit well with the theoretical predictions, which validates the pressure distribution provided by Willis (1966).

In addition to indentation force and contacting pressure, we also compare the contacting area between a spherical indenter and a prestretched elastomer obtained from theoretical predictions and FEM simulations, as shown in Figs. 8 and 9. The theoretical value of the eccentricity of the contacting area in Fig. 8 is given by Eq. (42). As expected, eccentricity increases monotonically from zero to one when the prestretch ratio λ_1/λ_2 is decreased from one to zero. It also clearly shows that the eccentricity does not only depend on the prestretch ratio λ_2/λ_1 as proposed by Gay (2000). Instead, the eccentricity of the contacting area depends on both principle prestretches λ_1 and λ_2 as shown in Fig. 8(a). It is noted that if both λ_1 and λ_2 are larger than one as shown in Fig. 8(b), it may be reasonable to assume the eccentricity is only a function of prestretch ratio λ_2/λ_1 as adopted in previous study (Gay, 2000; Zafiropoulou et al., 2016).

Normalized contacting area A/A_0 between a spherical indenter and a prestretched elastomer is plotted in different prestretched state in Fig. 9, where $A = \pi ab$ is calculated using Eq. (47) and $A_0 = \pi DR$ is the contacting area for non-prestretched case. It is noted that the normalized contacting area does not depend on indentation depth anymore. For arbitrary λ_1, the normalized contacting area decreases from one to zero as the prestretch ratio λ_1/λ_2 decreases from one to zero. As indicated in Eq. (47), the normalized contacting area is only a function of eccentricity e. Therefore, the normalized contacting area mainly depends on the prestretch ratio when λ_1 and λ_2 are much larger than one based on the results of Fig. 8(b).

4. Concluding remarks

In this article, we study the effects of prestretched state of an elastomer on its indentation measurement. Using surface Green's function, we have analytically derived the relationship between indentation force and indentation depth for both flat-ended cylindrical indenter and spherical indenter. Our results have shown that the existence of prestretches in an elastomer can dramatically impact its indentation measurements, and thus it is critical to take consider prestretches of an elastomer when conducting indentation experiments. In particular, for certain prestretch state, measured indentation modulus can approach zero for an elastomer with finite elastic modulus. The formula derived in the article will provide the basis for designing a new indentation method for measuring both elastic modulus and prestretches of an elastomer or soft biological tissue, which will also be one of our future research directions of the topic. In addition, the results presented in the article can also provide important insights into the understanding of the effects of prestretch on the contact, adhesion and friction of soft elastomers.

Acknowledgment

The work is supported by the ONR (grant number N00014-17-1-2056).

References

Amar, M.B., Goriely, A., 2005. Growth and instability in elastic tissues. J. Mech. Phys. Solids 53, 2284–2319.
Beatty, M., Usmani, S., 1975. On the indentation of a highly elastic half-space. Q. J. Mech. Appl. Math. 28, 47–62.
Beebe, D.J., Moore, J.S., Bauer, J.M., Yu, Q., Liu, R.H., Devadoss, C., Jo, B.-H., 2000. Functional hydrogel structures for autonomous flow control inside microfluidic channels. Nature 404, 588–590.
Biot, M.A., 1963. Surface instability of rubber in compression. Appl. Sci. Res. Section A 12, 168–182.
Biot, M.A., 1965. Mechanics of Incremental Deformations: Theory of Elasticity and Viscoelasticity of Initially Stressed Solids and Fluids, Including Thermodynamic Foundations and Applications to Finite Strain. Wiley.
Bower, A.F., 2009. Applied mechanics of solids. CRC press.
Briscoe, B., Fiori, L., Pelillo, E., 1998. Nano-indentation of polymeric surfaces. J. Phys. D 31, 2395.
Cai, S., Chen, D., Suo, Z., Hayward, R.C., 2012. Creasing instability of elastomer films. Soft Matter 8, 1301–1304.
Constantinides, G., Kalcioglu, Z.I., McFarland, M., Smith, J.F., Van Vliet, K.J., 2008. Probing mechanical properties of fully hydrated gels and biological tissues. J. Biomech. 41, 3285–3289.
Corcoran, S., Colton, R., Lilleodden, E., Gerberich, W., 1997. Anomalous plastic deformation at surfaces: nanoindentation of gold single crystals. Phys. Rev. B 55, R16057.
Dhaliwal, R.S., Singh, B.M., 1978. The axisymmetric Boussinesq problem of an initially stressed neo-Hookean half-space for a punch of arbitrary profile. Int. J. Eng. Sci. 16, 379–385.
Ebenstein, D., Pruitt, L., 2004. Nanoindentation of soft hydrated materials for application to vascular tissues. J. Biomed. Mater. Res. Part A 69, 222–232.
Ebenstein, D.M., Pruitt, L.A., 2006. Nanoindentation of biological materials. Nano Today 1, 26–33.
Filippova, L., 1978. Three-dimensional contact problem for a prestressed elastic body: PMM vol. 42, no. 6, 1978, pp 1080–1084. J. Appl. Math. Mech. 42, 1183–1188.
Fung, Y., 1991. What are the residual stresses doing in our blood vessels? Ann. Biomed. Eng. 19, 237–249.
Fung, Y., Liu, S., 1989. Change of residual strains in arteries due to hypertrophy caused by aortic constriction. Circ. Res. 65, 1340–1349.
Gay, C., 2000. Does stretching affect adhesion? Int. J. Adhes. Adhes. 20, 387–393.
Gong, J., Wu, J., Guan, Z., 1999. Examination of the indentation size effect in low-load Vickers hardness testing of ceramics. J. Eur. Ceram. Soc. 19, 2625–2631.
Goriely, A., Weickenmeier, J., Kuhl, E., 2016. Stress singularities in swelling soft solids. Phys. Rev. Lett. 117, 138001.
Green, A., Rivlin, R., Shield, R., 1952. General theory of small elastic deformations superposed on finite elastic deformations. In: Proceedings of the Royal Society of London A: Mathematical, Physical and Engineering Sciences. The Royal Society, pp. 128–154.
He, L., 2008. Elastic interaction between force dipoles on a stretchable substrate. J. Mech. Phys. Solids 56, 2957–2971.
Hong, W., Zhao, X., Suo, Z., 2009. Formation of creases on the surfaces of elastomers and gels. Appl. Phys. Lett. 95, 111901.
Hu, Y., You, J.-O., Auguste, D.T., Suo, Z., Vlassak, J.J., 2012. Indentation: a simple, nondestructive method for characterizing the mechanical and transport properties of pH-sensitive hydrogels. J. Mater. Res. 27, 152–160.
Hu, Y., Zhao, X., Vlassak, J.J., Suo, Z., 2010. Using indentation to characterize the poroelasticity of gels. Appl. Phys. Lett. 96, 121904.
Huang, Y.-P., Zheng, Y.-P., Leung, S.-F., 2005. Quasi-linear viscoelastic properties of fibrotic neck tissues obtained from ultrasound indentation tests in vivo. Clin. Biomech. (Bristol,. Avon) 20, 145–154.
Ma, Q., Clarke, D.R., 1995. Size dependent hardness of silver single crystals. J. Mater. Res. 10, 853–863.
Marcombe, R., Cai, S., Hong, W., Zhao, X., Lapusta, Y., Suo, Z., 2010. A theory of constrained swelling of a pH-sensitive hydrogel. Soft Matter 6, 784–793.
Nix, W.D., Gao, H., 1998. Indentation size effects in crystalline materials: a law for strain gradient plasticity. J. Mech. Phys. Solids 46, 411–425.
Ogden, R.W., 1997. Non-Linear Elastic Deformations. Courier Corporation.
Oyen, M.L., 2008. Poroelastic nanoindentation responses of hydrated bone. J. Mater. Res. 23, 1307–1314.
Oyen, M.L., 2010. Handbook of Nanoindentation: With Biological Applications. Pan Stanford Publishing.
Pharr, G., 1998. Measurement of mechanical properties by ultra-low load indentation. Mater. Sci. Eng. 253, 151–159.
Rausch, M.K., Kuhl, E., 2013. On the effect of prestrain and residual stress in thin biological membranes. J. Mech. Phys. Solids 61, 1955–1969.
Rho, J.-Y., Tsui, T.Y., Pharr, G.M., 1997. Elastic properties of human cortical and trabecular lamellar bone measured by nanoindentation. Biomaterials. 18, 1325–1330.
Silver-Thorn, M.B., 1999. In vivo indentation of lower extremity limb soft tissues. IEEE Trans. Rehabil. Eng. 7, 268–277.
VanLandingham, M.R., Villarrubia, J.S., Guthrie, W.F., Meyers, G.F., 2001. Nanoindentation of Polymers: An Overview, Macromolecular Symposia. Wiley-Blackwell, 111 River Street Hoboken NJ 07030-5774 USA, pp. 15–44.
Vannah, W.M., Childress, D.S., 1996. Indentor tests and finite element modeling of bulk muscular tissue in vivo. J. Rehabil. Res. Dev. 33, 239.
Willis, J., 1966. Hertzian contact of anisotropic bodies. J. Mech. Phys. Solids 14, 163–176.
Willis, J., 1967. Boussinesq problems for an anisotropic half-space. J. Mech. Phys. Solids 15, 331–339.
Zafiropoulou, V., Zisis, T., Giannakopoulos, A., 2016. Instrumented indentation of a non-equal biaxial prestretched hyperelastic substrate. Eur. J. Mech. A/Solids 58, 221–232.
Zamir, E.A., Taber, L.A., 2004. On the effects of residual stress in microindentation tests of soft tissue structures. J. Biomech. Eng. 126, 276–283.